







# Heart dysfunction in a rat model with autosomal recessive polycystic kidney disease

Nathalie Gayraud<sup>1</sup> , Maëlle Plawecki<sup>2,3</sup>, Céline Lauret<sup>2</sup>, Marc Fila<sup>4</sup> , Pierre Sicard<sup>2</sup> , Flore Duranton<sup>1</sup>, Juliana H. Boukhaled<sup>1</sup>, Irene Cortijo-Tejero<sup>1</sup>, Manuela Lotierzo<sup>2,3</sup> , Bernard Jover<sup>2</sup> , Jean-Paul Cristol<sup>2,3</sup> and Fabrice Raynaud<sup>2</sup> 

<sup>1</sup>RD Néphrologie, Montpellier, France

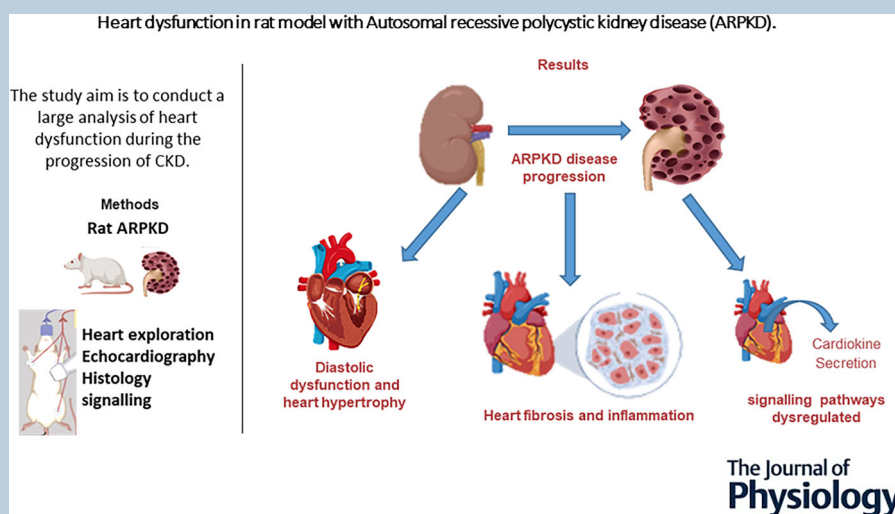
<sup>2</sup>PHYMEDEXP, Montpellier University, INSERM, CNRS, Montpellier, France

<sup>3</sup>Department of Biochemistry and Hormonology, University Hospital (CHU Lapeyronie) of Montpellier, Montpellier, France

<sup>4</sup>Department of Pediatric Nephrology, CHU Arnaud de Villeneuve, SORARE Montpellier University, Montpellier, France

Handling Editors: Bjorn Knollmann & Lewan Parker

The peer review history is available in the Supporting Information section of this article (<https://doi.org/10.1113/JP286364#support-information-section>).



**Abstract figure legend** Our results demonstrate a diastolic dysfunction in animals with severe kidney disease. Moreover, chronic kidney disease (CKD)-induced heart fibrosis and hypertrophy are associated with a dysregulation of cardiokine signalling in autosomal recessive polycystic kidney disease (ARPKD) animals. Created using BioRender.com.

**Abstract** Autosomal recessive polycystic kidney disease (ARPKD) is a congenital hepatorenal fibrocystic pathology and is one of the most significant childhood nephropathies leading to chronic kidney disease (CKD). While kidney damage has been well studied in this pathology, only a few studies have investigated specific cardiac damage during ARPKD. This study aimed to conduct a large analysis of heart dysfunction during the progression of CKD. ARPKD rats with the *Pkhd1* gene mutation (IVS35-2A>T) were monitored for CKD progression and heart dysfunction via echocardiography. Heart fibrosis was assessed using Sirius red staining, and cardiokines mRNA expressions in heart tissue were analysed. ARPKD rats exhibited increased blood pressure, cardiac hypertrophy and thickening of the left ventricular posterior wall, correlated with elevated plasma creatinine levels. Diastolic dysfunction was evident, shown by altered  $E/A$  and  $E/e'$  ratios, which worsened with CKD severity. Heart fibrosis correlated with renal dysfunction, and fibrosis signalling pathways were activated, marked by increased galectin-3, collagen-1, fibroblast growth factor 23, suppressor of tumorigenicity 2 (ST2) and soluble ST2 expression. Growth differentiation factor 15

levels rose with CKD progression, while Irisin levels decreased, negatively correlating with the  $E/e'$  ratio. This study highlights diastolic dysfunction, heart fibrosis, and hypertrophy in ARPKD rats with severe CKD. These cardiac changes are linked to dysregulation in cardiokine signalling, providing new insights into uraemia-induced heart failure in ARPKD

(Received 31 January 2024; accepted after revision 18 March 2025; first published online 12 April 2025)

**Corresponding author** F. Raynaud: PhyMedExp, IURC, 691 avenue doyen Giraud, 34090 Montpellier, France. Email: fabrice.raynaud1@umontpellier.fr

### Key points

- Autosomal recessive polycystic kidney disease (ARPKD) is a rare genetic disorder with a reduced life expectancy and a broad clinical spectrum including systemic hypertension, renal failure, portal hypertension, and renal and hepatic fibrosis.
- PCK rats have a spontaneous mutation in the *Pkhd1* gene, the same gene affected in human ARPKD. PCK rats develop renal and hepatic cysts and other manifestations of human ARPKD.
- Changes in heart tissue (fibrosis, hypertrophy) and diastolic dysfunction (decreasing  $E/A$  and increasing  $E/e'$  ratios) worsen with renal dysfunction in PCK rats.
- Heart dysfunctions are associated with a dysregulation of cardiokine signalling such as Irisin, in PCK rats.
- Irisin could be a new marker of diastolic function in ARPKD and chronic kidney disease patients.

## Introduction

Autosomal recessive polycystic kidney disease (ARPKD) has an estimated incidence of 1 in 20,000 and belongs to a group of congenital hepatorenal fibrocystic syndromes (Bergmann et al., 2006; Harris & Torres, 2009; Turkbey et al., 2009; Zerres et al., 1998). ARPKD is caused by mutations in the *PKHD1* gene, which encodes a large multi-domain integral membrane protein known as fibrocystin/polyductin (FPC) (Bergmann et al., 2004; Chinali et al., 2007, 2015) with poorly understood function. A recent paper revealed an implication of FPC in mitochondrial function and structure (Walker et al., 2023). Renal symptoms are characterized by kidney enlargement in childhood, hypertension and varying degrees of renal dysfunction. Hypertension is the most common and earliest finding of both autosomal-dominant and -recessive variants of polycystic kidney disease (PCK) (Capisonda et al., 2003; Gabow et al., 1990) but the causal factors of hypertension in ARPKD remain unclear. Volume overload associated with poor renal function has been suggested (Gagnadoux et al., 1989) as well hyponatraemia (Kaplan et al., 1989). A case report of hypertensive neonates with low renin levels (Field, 1985) further raises questions about the role of the renin-angiotensin system in this hypertension. Alternatively, hypertension could be linked to cardiac dysfunction that is known to play a major role in the development of left ventricular hypertrophy (Klein et al., 2020). The significant increase in cardiac workload could be associated with sub-

clinical abnormalities of systolic mechanical function, concentric remodelling and left ventricular hypertrophy before impairment of ejection fraction (Chinali et al., 2007, 2019). Furthermore, previous evidence from rat models of ARPKD has shown a significant temporal relationship between cyst development, hypertension and left ventricular hypertrophy (Phillips et al., 2007). The clinical phenotypes of ARPKD can be quite variable, and biomarkers of disease progression are not available (Benz & Hartung, 2021).

Our study aimed to characterize the structural and functional heart abnormalities during the progression of chronic kidney disease (CKD) induced by ARPKD in a rat model (PCK) previously described (Lager et al., 2001) and to explore the molecular pathways involved in this dysfunction. We focused on inflammatory biomarkers related to the diagnosis and management of heart failure (Castiglione et al., 2022): pro-collagenic factors such as galectin-3, interleukin (IL)-33/suppressor of tumorigenicity 2 (ST2)/soluble ST2 (sST-2) systems, growth differentiation factor (GDF)-11 and insulin-like growth factor-1 (IGF1), markers of myocardial hypertrophy, left ventricular fibrosis and cardiac remodelling (Fontana Estevez et al., 2022; Plawecki et al., 2018). In addition fibroblast growth factor (FGF) 23/FGF23 receptors/Klotho pathway, GDF15, Irisin, Apelin, FGF21 and follistatin-like protein 1 (FSTL1), which have been previously involved in cardiac remodelling, were determined (El-Armouche et al., 2011; Furukawa et al., 2021).

## Methods

### Ethical approval

The present experiment complied with European and French laws (Agreement D34-172-25 and 1562-18348) and with the *Guide for the Care and Use of Laboratory Animals* published by the National Institutes of health (National academies Press US, 8th edition, 2011). Rats were housed in climate-controlled conditions with a 12h light-dark cycle at room temperature (Referral no. = 1457-13685). They had free access to standard diet (A04, UAR is French safe lab) and water. All animals were killed by a lethal injection of pentobarbital (200 mg/kg i.p.), after the last blood pressure measurement was carried out under gas sedation with isoflurane (2% in O<sub>2</sub>), without the animal waking up. For euthanasia, we used pentobarbital (Euthasol).

**Animal model.** Male Sprague-Dawley rats (control group) and ARPKD-developing Sprague-Dawley rats (ARPKD group, PCK rat strain) with splicing mutation (IVS35-2A→T) in *Pkhd1* gene that causes skipping of the 157 bp exon 36 were used and followed for CKD progression kinetics at 3, 6–7 and 9–11 months (3M, 6M and 9M). All animals were obtained from Charles River Laboratories (Charles River's facility in Lyon, France).

The first animals sampled were not analysed by cardiac ultrasound, but had biochemical and histological results indicating cardiac damage. Therefore, ultrasound monitoring of the following rats was performed (Fig. 1). Uneven group sizes resulted from breeding challenges, small litter sizes, and age-related mortality in the rat colony, particularly for animals aged 9–11 months.

At the end of the experiment, rats were anaesthetised with 2% isoflurane, and lidocaine chloridrate (0.5%

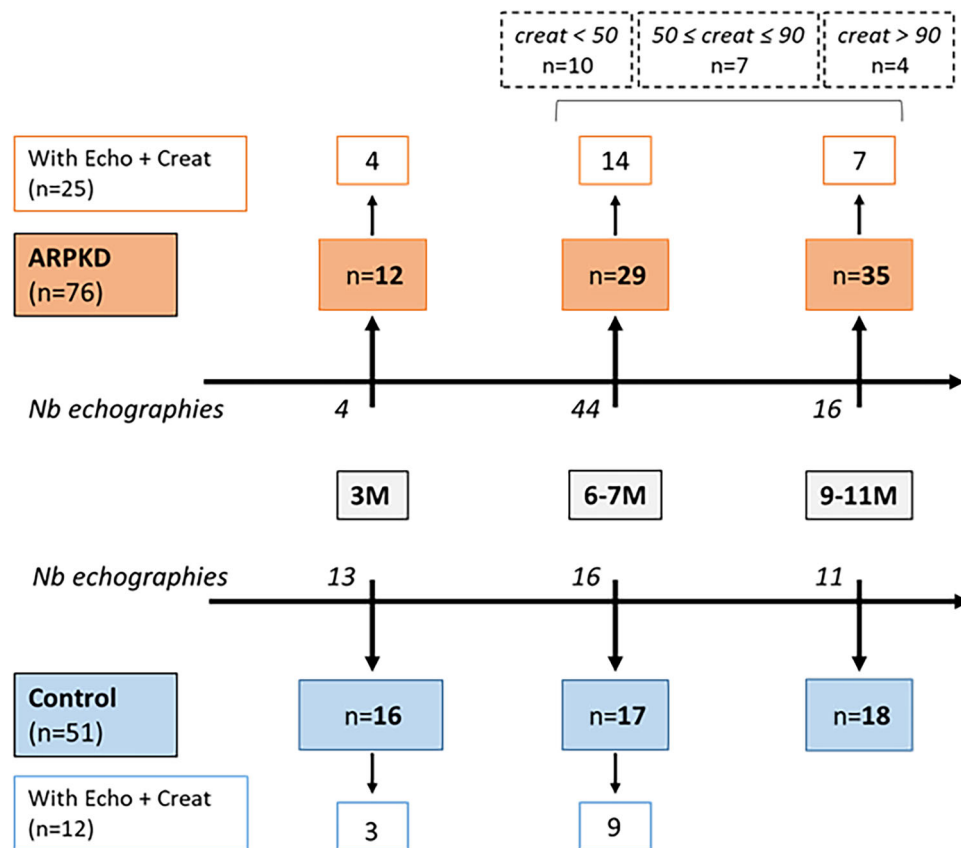


**Figure 1. Study design**

A total of 76 ARPKD (orange) and 51 controls (blue) rats were followed until the age of 3–11 months old (grey). Animals were assessed or sacrificed after 3 months (3M), 6–7 months (6M) or 9–11 months (9M). The number of sacrificed animals are shown by a filled orange (ARPKD) or blue (Control) rectangle at each point of age. The number of total cardiac echography is shown in black (Nb echographies). The number of cases with both plasma creatinine level (CKD severity) and cardiac echography at different time points is shown in an open orange rectangle (ARPKD) and open blue rectangle (Control). Dashed rectangles represent the number of echocardiography related to the CKD severity. [Colour figure can be viewed at [wileyonlinelibrary.com](http://wileyonlinelibrary.com)]

**Table 1. Plasma analysis of biological parameters, cardiac natriuretic peptides and arterial pressure in ARPKD rats**

Analysed parameter	Control average		ARPKD 3M		ARPKD 6–7M		ARPKD 9–11M		<i>P</i>
	<i>n</i>	Mean ± SEM	<i>n</i>	Mean ± SEM	<i>n</i>	Mean ± SEM	<i>n</i>	Mean ± SEM	
Creatinine (μM)	31	37 ± 2 (a)	11	27.5 ± 1.7 (b)	20	42 ± 3.5 (c)	27	164 ± 39 (a. c. b)	<b>0.0002</b>
Urea (mg/dl)	31	6.3 ± 0.3 (a)	11	5.6 ± 0.5 (b)	20	6 ± 0.5 (c)	21	19 ± 4 (a. b. c)	<b>0.0001</b>
ALAT (UI/l)	19	49.5 ± 4.5 (a)	5	55 ± 4 (b)	11	33 ± 4	9	24 ± 3.5 (a. b)	<b>0.0015</b>
PAL (UI/l)	24	122 ± 10.5	6	174.5 ± 36.5	8	125.5 ± 8	6	127.0 ± 17.0	<b>0.996</b>
Calcium (mmol/l)	31	2.4 ± 0.05	11	2.5 ± 0.05	21	2.5 ± 0.02	17	2.5 ± 0.05	<b>0.202</b>
Phosphore (mmol/l)	31	2.2 ± 0.1	11	2.2 ± 0.2	20	2.25 ± 0.07	17	2.55 ± 0.37	<b>0.501</b>
Sodium (mmol/l)	31	135.5 ± 1.6 (a)	11	133.5 ± 2.7 (b)	21	140 ± 1	17	142 ± 1.50 (a. b)	<b>0.0295</b>
Potassium (mmol/l)	29	5.6 ± 1.3	11	6.1 ± 1.2	20	5.5 ± 1.2	20	6 ± 2	<b>0.897</b>
ANP (heart RNA expression)	24	0.07 ± 0.02 (a)	5	0.2 ± 0.15	17	0.2 ± 0.05	30	0.5 ± 0.1 (a)	<b>0.0003</b>
BNP (heart RNA expression)	28	0.25 ± 0.02	6	0.30 ± 0.05	18	0.30 ± 0.015	31	0.30 ± 0.02	<b>0.18</b>
Arterial Pressure (mmHg)	15	122.5 ± 3.0 (a)	5	131 ± 7.5	13	125 ± 5.0	11	154 ± 6.5 (a)	<b>0.0002</b>

The group mean values with the same letters (a, b, c) are significantly different results. Heart ANP and BNP gene expression was normalized to *RPLPO* expression. Control average: control rats were pooled together because no significant difference could be evidenced according to the age (Fig. 5). ALAT, alanine aminotransferase; ANP, atrial natriuretic peptide; BNP, B type natriuretic peptide; PAL, plasmatic alkaline phosphatase.

xylocaine) was injected locally subcutaneously. Gas inhalation was initiated in an anaesthesia chamber and maintained using a mask during the procedure. The skin was cleansed with 10% betadine and incised at the carotid artery access site. A catheter was inserted into the right carotid artery to measure blood pressure and take blood samples. The left ventricle (LV) including septum was removed, weighed separately and cut into pre-defined pieces for RNA and protein extractions and histology. Arterial blood was collected in a heparinized-tube, centrifuged at 4°C and then plasma was stored at –80°C for biological parameter analysis (Table 1).

### Echocardiography and speckle-tracking analysis

High-resolution echocardiography (VisualSonics/Fujifilm, with a 20-MHz MS250D ultrasound probe) was performed under anaesthesia by 2% isoflurane inhalation at 37°C. The ECG and respiratory rate were monitored. Using standard VisualSonics VevoLab software for two-dimensional (2D) strain analysis. For the kinetic study, animals were monitored at different time points (3, 6–7 and 9–11 months) and all results are presented in Table 2. For analysis according to severity, only the final ultrasound was considered. The mitral valve (MV) leaflet was visualized, and mitral flow (MV flow and MV tissue Doppler) were assessed with the apical four-chamber B-mode view and recorded using pulsed-wave Doppler. Wall thicknesses as well as end-systolic and end-diastolic LV dimensions were measured according to American Physiological Society guidelines, as applied to rats (Lindsey et al., 2018). LV wall thickness was measured at the level of intraventricular septum and posterior wall. LV

volume was calculated from Simpson's method of disks, and ejection fraction was determined from the following formula: (end-diastolic LV volume – end-systolic LV volume)/(end-diastolic LV volume).

We specifically used left atrial area, isovolumetric relaxation time, the early filling peak (E wave)-to-late diastolic filling peak (A wave) ratio (*E/A*), the early diastolic mitral annular velocity (*E'*) and the ratio (*E/E'*) to determine the diastolic function index (Schnelle et al., 2018; Sicard et al., 2019). Offline image analyses were performed using VisualSonics (Poitou, France) VevoLab 3.1.0 software. We used the Speckle Tracking Echocardiography (STE) software with semi-automated border tracking in the parasternal long-axis view for analysis. First, the user places a number of tracking points on the endocardial and epicardial borders. During STE analysis, the LV is automatically divided into six segments. We analysed global longitudinal peak strain (longi pK%), the systolic strain rate (longi rate pk (1/s)), the early diastolic strain rate (SRE), and calculated the diastolic marker (*E/SRE*).

### Analysis of mRNA expression by real-time PCR

Immediately after removal and weighing the left ventricle, a pre-defined section was frozen in RNA Later solution (Thermo Fisher Scientific, Waltham, MA, USA). Tissues were then dissociated in RLT buffer using a FastPrep Homogenizer (MP Biomedicals, France). Reverse transcription reactions were performed on 500 ng total RNA using the reverse transcription Takara Kit (Takara Bio Europe-France) and real-time quantitative PCR was done with the use of the Lightcycler 480 II real time PCR

**Table 2. Heart Ultrasound analysis at different ages of the pathology**

Parameter	Control average		ARPKD 6–7M		ARPKD 9–11M		P
	n	Mean ± SEM	n	Mean ± SEM	n	Mean ± SEM	
E (mm/s)	28	740 ± 32	44	695 ± 19.5	16	745.5 ± 45.5	0.932
A (mm/s)	28	506.5 ± 26.5 (a)	43	510 ± 23.5 (b)	16	648.5 ± 64 (a. b)	0.0195
E/A	28	1.5 ± 0.1 (a)	43	1.45 ± 0.05	16	1.2 ± 0.1 (a)	0.0241
Dcel (ms)	28	28.0 ± 1.7	41	29.0 ± 1.5	15	26.8 ± 1.7	0.898
E/SRE	26	210.2 ± 22	41	211.5 ± 16	12	200.5 ± 26	0.801
e'	28	41.3 ± 3 (a)	44	37.3 ± 2	16	30.2 ± 3.5 (a)	0.0472
E/e'	27	19.1 ± 1.5 (a)	44	20.7 ± 1.1 (b)	16	28.9 ± 3.2 (a.b)	0.0053
EF	27	59.3 ± 1.7 (a)	44	55.7 ± 1.2 (b)	16	46.9 ± 3.1 (a.b)	0.0338
IVS.d (mm)	13	2.15 ± 0.1	26	2.15 ± 0.06	9	2.34 ± 0.15	0.388
IVS.s (mm)	13	3.23 ± 0.15	26	3.2 ± 0.1	9	3.5 ± 0.1	0.278
LVID.d (mm)	13	8.2 ± 0.3	26	7.3 ± 0.25	9	7.5 ± 0.5	0.422
LVID.s (mm)	13	5.2 ± 0.3	26	4.7 ± 0.2	9	4.4 ± 0.4	0.201
LVPW.d (mm)	13	2.3 ± 0.1	26	2.2 ± 0.06	9	2.6 ± 0.3	0.359
LVPW.s (mm)	13	3.3 ± 0.1	26	3.0 ± 0.1 (b)	9	3.7 ± 0.3 (b)	0.0266
longi pk%	28	−16.3 ± 1.2	42	−15.4 ± 0.6	12	−16.4 ± 1.4	0.726
longi rate pk (1/s) (s <sup>−1</sup> )	28	−4.2 ± 0.3	42	−4.1 ± 0.15	12	−4.1 ± 0.3	0.399
SRE (s <sup>−1</sup> )	28	4.2 ± 0.4	41	3.9 ± 0.3	12	4.2 ± 0.5	0.955

For each kinetic point (3, 6–7 and 9–11 months), we performed an ultrasound analysis for all animals. The group mean values with the same letters (a, b, c) are significantly different. Control average: control rats were pooled together because no significant difference could be evidenced according to the age. A, Doppler mitral active filling with atrial systole (late wave); Dce, E deceleration; e', diastolic mitral annular velocity, a tissue doppler parameter; E, Doppler mitral passive filling of the ventricle late wave active; EF, ejection fraction; IV, interventricular septum thickness; longi pk%, global longitudinal peak strain; longi rate pk (1/s), longitudinal systolic strain rate; LVID, left ventricular internal diameter; LVPW, left ventricular posterior wall thickness (s: systolic and d: diastolic); SRE, early diastolic strain rate.

instrument (Roche-To determine whether the values are constant over time in the control groups, we performed a statistical analysis for each of the parameters. France). Primer pairs were generated using NCBI primer design application and were designed to span an exon–exon junction (Integrated DNA Technologies, Leuven, Belgium). Forward and reverse primers sequences were used at specific annealing temperature. Expression levels were determined with the LightCycler analysis software (version 3.5) relative to standard curves. Data were represented as the mean level of gene expression relative to the expression of the reference housekeeping gene *RPLPO*. We used the method of Pfaffl (2001) for real time PCR calculation:

$$\text{Ratio} = \frac{(E_{\text{target}})^{\Delta\text{CP}_{\text{target}}(\text{control-sample})}}{(E_{\text{ref}})^{\Delta\text{CP}_{\text{ref}}(\text{control-sample})}}$$

### Histochemical staining

For cardiac collagen staining, a pre-defined section of the LV was formalin-fixed, paraffin-embedded, and 3–5 µm slices were cut for histological analysis. The collagen volume fraction was determined by Sirius red staining, as previously described (Plawecki et al., 2024).

### Statistics

Quantitative data were expressed as means ± SEM. Statistical analyses were performed using two factor analysis of variance (ANOVA) and *post hoc* comparisons were performed by means of Fisher's protected least significant difference (PLSD) test using GraphPad Prism 8 software (GraphPad Software, San Diego, CA, USA). A *P*-value of <0.05 was considered significant.

In a first step, a time-based analysis was performed (3M, 6–7M, 9–11M).

Since no significant difference could be evidenced in control rats according to the age, control rats were pooled together (Table 3). In a second step, analyses were performed according to kidney disease severity. We defined three groups of CKD severity, in analogy with CKD classification in patients (Anon, 2013): plasma creatinine <50 µM (no or mild CKD; <30% of kidney function lost compared to control animals); plasma creatinine from 50 to 90 µM (moderate CKD; 30–70% of kidney function lost); and plasma creatinine >90 µM (severe CKD; >70% of kidney function lost). Analyses according to kidney disease severity were performed with non-parametric ANOVA. We also performed Pearson linear correlations between echocardiography, heart RNA expressions and markers, followed by variable



**Table 3. Biological parameters analysed were constant values in healthy animals**

	Means of controls kinetic			<i>P</i>
	Control 3M	Control 6M	Control 9M	
Arterial pressure (mmHg)	122 ± 5.5	123 ± 3.5	122 ± 6	0.963
SRE = pk (1/s) en s-1	4.8 ± 2.5	3.7 ± 2	4.5 ± 0.6	0.362
<i>E</i> (mm/s)	765 ± 144	716 ± 96	745 ± 85	0.539
<i>A</i> (mm/s)	547 ± 122	502 ± 186	597 ± 201	0.387
<i>E/A</i>	1.43 ± 0.3	1.6 ± 0.5	1.7 ± 0.4	0.973
Dcel (ms)	27 ± 10	29 ± 8	31 ± 10	0.711
<i>E/SRE</i>	188 ± 87	232 ± 89	179 ± 53	0.371
<i>e'</i>	38 ± 12	44.5 ± 17	37.6 ± 12.5	0.372
EF	61 ± 10	57.5 ± 7.5	62 ± 7.5	0.46
<i>E/e'</i>	21.5 ± 6.2	16.6 ± 5.5	22.5 ± 9.5	0.392
IVS;d	2.20 ± 0.4	2.1 ± 0.3	2.0 ± 0.2	0.677
IVS;s	3.35 ± 0.7	3. ± 0.5	3.3 ± 0.2	0.115
LVID;d	7.3 ± 0.6	8.8 ± 0.7	8.0 ± 0.6	0.378
LVID;s	4.4 ± 0.8	5.8 ± 0.8	4.6 ± 0.2	0.314
LVPW;d	2.4 ± 0.3	2.3 ± 0.3	2.5 ± 0.2	0.463
LVPW;s	3.4 ± 0.5	3.2 ± 0.3	3.6 ± 0.7	0.279
longi pk%	17.8 ± 7.5	15.0 ± 5.2	18.2 ± 2.1	0.823
longi-rate-pk (1/s)	5.0 ± 2	3.5 ± 1.2	4.2 ± 0.1	0.258
Sirius red	2.1 ± 0.6	3.8 ± 0.3	4.4 ± 1.4	0.0576
GDF15	1.38E-04	2.16E-04	2.28E-04	0.999
ANP	4.02E-02	5.70E-02	1.96E-01	0.401
BNP	1.68E-01	2.26E-01	3.04E-01	0.129
IL-33	2.41E-03	2.59E-03	2.82E-03	0.709
ST2	1.40E-04	8.68E-05	1.03E-04	0.39
sST2	3.41E-04	3.37E-04	3.29E-04	0.994
TNFα	3.45E-04	3.26E-04	4.14E-04	0.518
TGFB1	5.30E-03	6.09E-03	6.75E-03	0.599
IL-6	4.80E-05	3.10E-05	2.91E-05	0.536
Creatinine (mM)	37	35	41	0.727
Urea mg/dL	6.45	5.7	7.5	0.332
ALAT (IU/l)	56	35	26.2	0.876
PAL (IU/l)	125	124.5	154.2	0.771
Ca <sup>2+</sup> (mmol/l)	2.25	2.5	2.5	0.254
P (mmol/l)	2.1	2.4	1.9	0.681
Na <sup>+</sup> (mmol/l)	134.5	137.5	141.5	0.784
K <sup>+</sup> (mmol/l)	5.9	6.1	5.7	0.792
<i>FSTL1</i>	4.49E-04	3.00E-04	4.08E-04	0.863
<i>GDF11</i>	2.06E-03	2.79E-03	1.94E-03	0.981
<i>Irisin</i>	2.65E-02	2.54E-02	2.38E-02	0.773
<i>FGF21</i>	3.37E-04	3.52E-04	2.97E-04	0.582
<i>Decorin</i>	1.04E-01	1.02E-01	1.10E-01	0.85
<i>FGF23</i>	3.33E-05	5.07E-05	1.78E-05	0.947
<i>IL-15</i>	2.45E-03	2.13E-03	1.95E-03	0.202
<i>LIF</i>	2.25E-05	2.94E-05	2.91E-05	0.81
<i>IL8</i>	4.29E-04	4.30E-04	6.25E-04	0.668
<i>IL10</i>	4.13E-04	4.93E-04	4.80E-04	0.631
<i>Apelin</i>	2.25E-03	2.03E-03	1.56E-03	0.203
<i>IGF1</i>	1.43E-02	1.04E-02	1.32E-02	0.915

To determine whether the values are constant over time in the control groups, we performed a statistical analysis for each of the parameters. No significant differences were found in the parameters analysed.

**Table 4. Heart ultrasound analysis as a function of CKD severity**

Parameter	Control average	ARPKD <50	ARPKD 50–90	ARPKD >90	P
n (animals)	13	10	7	4	
E (mm/s)	740 ± 32	730 ± 136	750.5 ± 227	743 ± 120	0.965
A (mm/s)	506.5 ± 26.5 (a)	583 ± 193	625 ± 315	660 ± 139	0.708
E/A	1.5 ± 0.1 (a)	1.4 ± 0.5	1.3 ± 0.5	1.1 ± 0.1 (a)	0.026
Dcel (ms)	28 ± 1.7	30.4 ± 10	28 ± 9	34.5 ± 3	0.954
e'	41 ± 3 (a)	45.5 ± 19.5 (a)	29 ± 9.5	19 ± 4.5 (a)	0.0461
EF	59 ± 1.5 (a)	57 ± 10.5	49 ± 9.5	61.5 ± 5.5	0.954
E/e'	19 ± 1.5 (a)	18 ± 7.5 (b)	28 ± 10.5	41.5 ± 15 (a, b)	0.0036
IVS-d (mm)	2.1 ± 0.1	2.2 ± 0.4	2.3 ± 0.1	2.25 ± 0.5	0.656
IVS-s (mm)	3.2 ± 0.1	3.4 ± 0.3	3.4 ± 0.2	3.6 ± 0.4	0.855
LVID-d (mm)	8.2 ± 0.3	8 ± 1	7 ± 1	8 ± 1.7	0.999
LVID-s (mm)	5.2 ± 0.3	4.9 ± 1	4.4 ± 1.2	4.8 ± 1.4	0.945
LVPW-d (mm)	2.3 ± 0.1	2.0 ± 0.5 (a)	3.3 ± 1.5 (a)	2.7 ± 0.4	0.0387
LVPW-s (mm)	3.3 ± 0.1	3.1 ± 0.7	4.0 ± 2	3.9 ± 0.5	0.662
E/SRE	210 ± 22	179 ± 39	184 ± 38.5	222.5 ± 19	0.999
longi pk%	−16.3 ± 1.2	−18.6 ± 1.2	−17.9 ± 2.3	−11.25 ± 1.1	0.563
longi rate pk (1/s) (s <sup>−1</sup> )	−4.2 ± 0.3	−4.7 ± 0.2 (a)	−4.4 ± 0.6	−2.3 ± 0.2 (a)	0.037
SRE (s <sup>−1</sup> )	4.2 ± 0.4	5.6 ± 1.2	4.7 ± 0.8	3.4 ± 0.5	0.581

The group mean values with the same letters (a, b, c) are significantly different. A, Doppler mitral active filling with atrial systole (late wave); Dce, E deceleration; e', diastolic mitral annular velocity, a tissue doppler parameter; E, Doppler mitral passive filling of the ventricle early wave; EF, ejection fraction; IV, interventricular septum thickness; longi pk%, global longitudinal peak strain; longi rate pk (1/s), systolic strain rate; LVID, left ventricular internal diameter; LVPW, posterior wall of the left ventricle (s: systolic and d: diastolic); SRE, early diastolic strain rate.

clustering, in ARPKD rats with echocardiography ( $n = 36$ ). Correlations are displayed as a heatmap where values are represented by coloured gradient of red (1) to blue (−1) and variables are organized according to the clustering dendrogram. We identified six clusters of variables demonstrating high within-cluster correlations and comparable patterns of association with other variables. Interestingly, each cluster comprised ECG, mRNA and phenotypic markers.

## Results

### Autosomal recessive polycystic kidney disease progression

In ARPKD rats, we analysed the change in biological parameters over time to determine the progression of the pathology. Plasma creatinine and urea levels indicated a progressive decline in renal function up to 9–11 months (Table 1). Blood pressure analysis revealed that 9-month-old ARPKD rats had significantly higher arterial pressure (Control:  $122.5 \pm 3.0$  vs. ARPKD 9M:  $154.2 \pm 6.5$  mmHg, Table 1).

Since the development of the hepatorenal fibrocystic pathology is expected in ARPKD rats, hepatic parameters were examined. No differences in plasmatic alkaline phosphatase (PAL) levels were observed between the

control and ARPKD animals throughout the study period. The alanine aminotransferase (ALAT) levels decreased and were significantly different in 9-month-old ARPKD rats compared to control (Table 1).

When measuring electrolyte imbalances during the progression of CKD, no differences in the calcaemic, phosphataemia and kaliaemia were detected. However, natraemia was increased in the 9-month-old ARPKD group compared to control (Table 1) and cardiac expression of atrial natriuretic peptide (ANP) was also increased in these animals. We did not detect any change in cardiac expression of B type natriuretic peptide (BNP) (Table 1).

### Cardiac structural and functional alterations during the course of ARPKD

Left ventricular posterior wall thickness in diastole (LVPW-d) increased both over time and with CKD severity in ARPKD rats, and a similar trend was observed for LVPW during systolic events (LVPW-s) (Tables 2 and 4). In contrast, echocardiographic analysis revealed no reduction in left ventricular internal diameter (LVID) during systole and diastole in ARPKD rats, and inter-ventricular septum (IV) thickness was unaltered (Tables 2 and 4).

ARPKD animals at all ages presented a lower body weight (BW) than the control animals (Fig. 2A) and the heart weight index was higher in 6- and 9-month-old ARPKD rats compared with their respective controls (Fig. 2B). We did not observe any difference in heart weight index or arterial pressures in the ARPKD model in relation to the severity of CKD (Figs 2C and 2D).

LV diastolic function was assessed by measuring the velocities of the early (*E*) and late (*A*) mitral inflow peak and the *E/A* ratio was calculated. Left ventricular filling index (*E/e'*) was determined by tissue Doppler imaging. The tissue Doppler velocity *e'* (mm/s) dramatically decreased according to CKD severity or time course (Tables 2 and 4). The mitral flow (*A*) significantly increased with age but only a trend was observed with CKD severity (Tables 2 and 4). Decrease in *E/A* and *e'* and increase in *E/e'* clearly indicate a progressive LV diastolic dysfunction during the course of the CKD (Tables 2 and 4).

LV systolic function was assessed by ejection fraction and global longitudinal strain. We found an increase in the

*E*/early diastolic strain rate (SRE) ratio in the ARPKD > 90 group, which was not significant, certainly due to a limited sample size and statistical power ( $n = 4$ , Table 2).

The global longitudinal strain (longi pk%) and SRE tended to decrease with CKD severity but did not show significant differences (Table 4) and we found no difference over time (Table 2). The systolic strain rate (longi rate pk 1/s) was decreased in the ARPKD animals with severe CKD but not associated with age (Tables 2 and 4). Ejection fraction (EF) significantly decreased during the time course of ARPKD disease (Table 2) but not with the severity of CKD (Table 4).

### Heart fibrosis in the ARPKD animal

To assess heart fibrosis, Sirius red staining was performed on heart sections. At 3 and 6 months, we observed no differences in the surface area of stained tissue between control and ARPKD animals (Fig. 3A). However, in the ARPKD 9-month group, we detected a significant increase in heart fibrosis (Fig. 3A) but no change of collagen-1

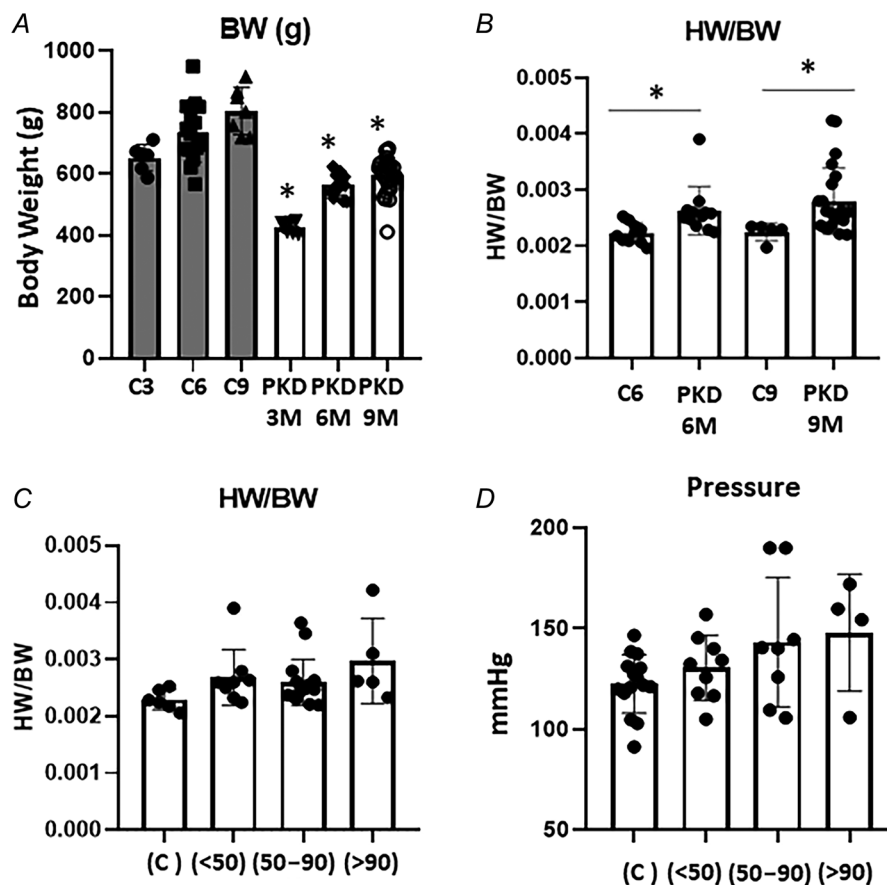


**Figure 2. Body and heart weights and pressure values**

A, body weight (g) for control animals (C 3, 6, 9 months) and for PKD animals (PKD 3, 6, 9 months) at the end of experiment. B, heart weight (HW)/body weight (BW) ratio at 6 and 9 months of age. C, ratio HW/BW as a function of CKD severity. D, arterial pressure in function of the CKD severity (mmHg). \*Significant difference,  $P < 0.05$ . PKD, polycystic kidney disease.



expression (Fig. 3D). There was, however, an increase of galectin-3 expression at 3 and 9 months for ARPKD rats compared with controls (Fig. 3F). Interestingly, analysing of Sirius red staining in relation to CKD severity, showed a progressive increase in fibrosis (Fig. 3B and C). Notably, ARPKD animals with severe kidney disease exhibited increased expression of collagen-1 and galectin-3 (Fig. 3E and G).

### Heart remodelling signalling pathways

We then assessed the expression level of genes potentially involved in progressive renal dysfunction. We first analysed the signalling pathway involved in heart hypertrophy, by focusing on the fibroblast growth factor 23 (FGF23)/Klotho system. Interestingly, we observed a progressive increase in the expression of FGF23 (Fig. 4A) without any changes in fibroblast growth factor receptor (FGFR) 4 expression (Fig. 4C) while FGFR2 progressively decreased with the severity of CKD (Fig. 4D). We did not observe an overexpression of the gene for Klotho (Fig. 4B), which acts as a co-receptor to enhance the binding affinity to FGF23 receptors (FGFR).

Heart remodelling and dysfunction is usually associated with overexpression of natriuretic peptides and local

inflammation. Surprisingly, we did not find significant changes in ANP and BNP expression with respect to the severity of CKD, although a dramatic increase in ANP expression was observed in some ARPKD rats (Fig. 5A and B). We found an increase in the expression of ANP in the 9-month-old ARPKD group (Table 1).

A dysregulation of the inflammatory pathway was observed with a significant increase in IL-6 expression in animals with the most severe CKD, while the anti-inflammatory cytokine IL-10 significantly decreased (Table 5). Leukaemia inhibitory factor (LIF), which belongs to the IL-6 family but has a protective effect on the myocardium, was increased in rats with severe CKD. LIF has also been shown to contribute to cardiac repair (Zouein et al., 2013). Surprisingly, the proinflammatory factor TNF- $\alpha$  decreased in ARPKD rats with severe CKD (Table 5). Similarly, the pro-fibrotic factor TGF- $\beta$ 1 exhibited decreased expression in the hearts of animals with severe CKD (Table 5).

Other signalling pathways associated with myocardial fibrosis were explored, including the mRNA expression of protein suppression tumorigenicity 2 (ST2), its soluble form (sST2), and interleukin-33 (IL-33) in the heart. We observed an increase in ST2 and sST2 expression in animals with severe CKD (Fig. 6A and B), as well as

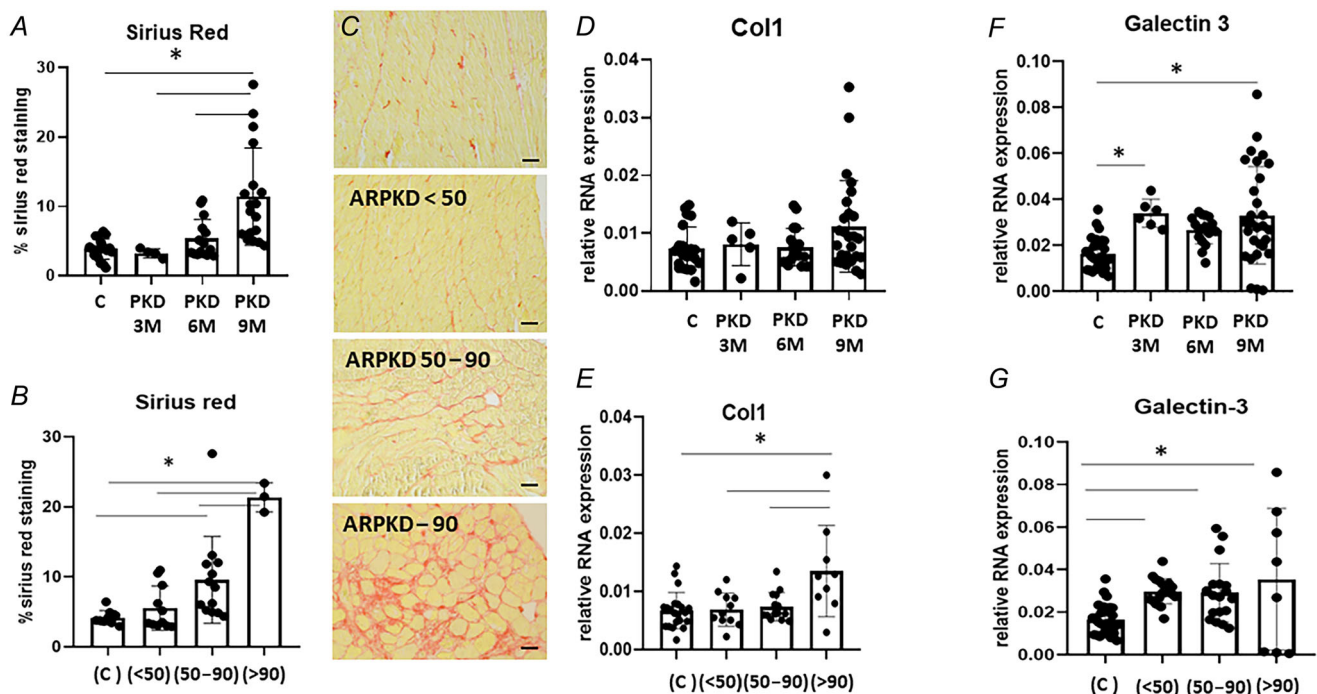


**Figure 3.** ARPKD rats present heart fibrosis

A, Sirius red staining on heart section as a function of age. B, Sirius red staining on heart section as a function of CKD severity (scale bar: 200  $\mu$ m). C, representative images of Sirius red-stained kidney sections from ARPKD rats classified according to CKD severity. D, collagen-1 gene expression in the heart as a function of age. E, collagen-1 gene expression in the heart as a function of CKD severity. F, galectin 3 gene expression in the heart as a function of age. G, galectin 3 gene expression in the heart as a function of CKD severity (gene expression was normalized to *RPLPO* expression). \*Significant difference,  $P < 0.05$ . [Colour figure can be viewed at [wileyonlinelibrary.com](http://wileyonlinelibrary.com)]

a decrease in the fibrotic inhibitory proteins IL-33 and decorin (Fig. 6D and E).

The expression of growth/differentiation factor-15 (GDF15), which is known to be overexpressed during cardiac damage, increased progressively with CKD severity and fibrosis progression (Fig. 6C). GDF11 and

the fibroblast growth factor FGF21 exhibited overexpression during the early stages of kidney disease (rats with creatinine levels <50 and between 50 and 90  $\mu\text{mol/l}$ ), but their expression did not change significantly in the severe stage. FSTL1, a protein that appears to have a cardioprotective role, exhibited overexpression in severe

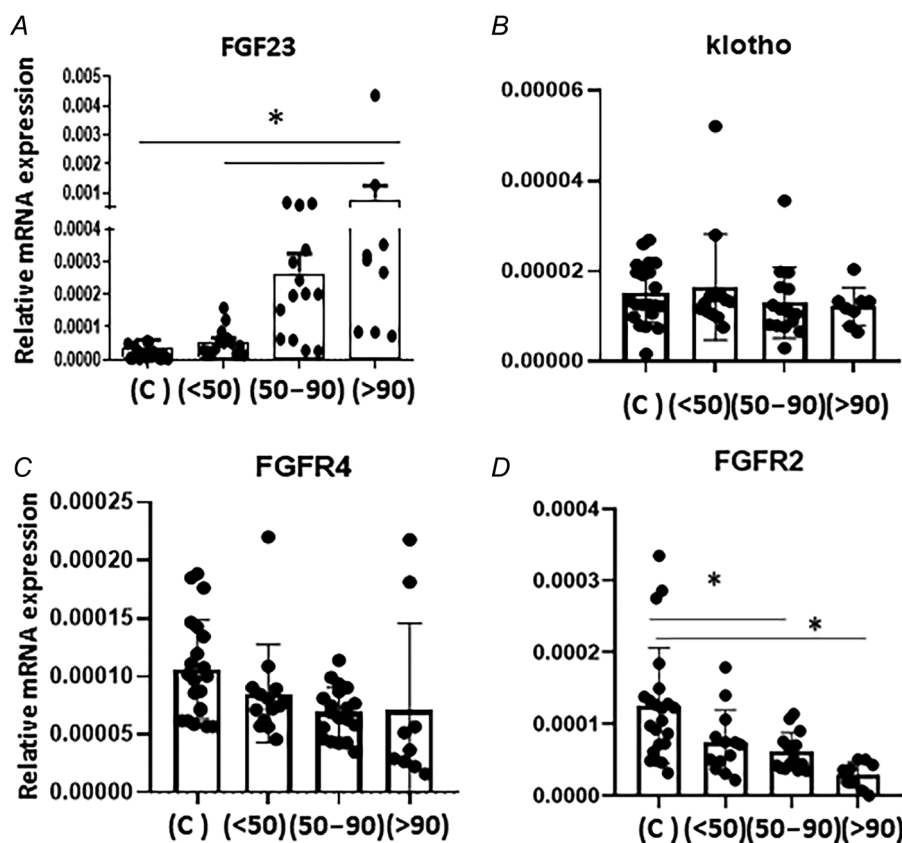


**Figure 4.** Heart hypertrophy signalling in the ARPKD rats. FGF23 (A), Klotho (B), and the receptors FGFR4 (C) and FGFR2 (D) gene expression in the heart as a function of CKD severity. Gene expression was normalized to *RPLPO* expression. \*Significant difference,  $P < 0.05$ .

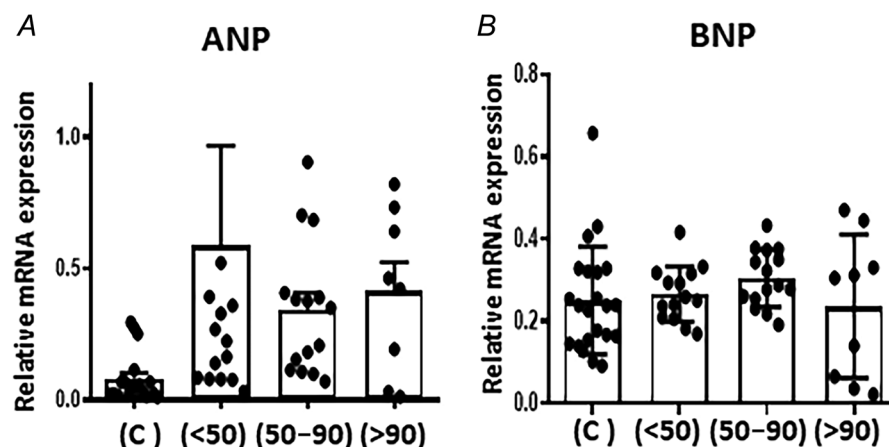


**Figure 5.** ANP (A) and BNP (B) gene expression in the heart as a function of CKD severity. Gene expression was normalized to *RPLPO* expression.

**Table 5. ARPKD rats present inflammatory state and cardiokine expression dysregulation**

<i>n</i>	Control 24	ARPKD <50 14	ARPKD 50–90 15	ARPKD >90 9	<i>P</i>
<i>IL6</i>	4.0E-05 ± 8.0E-06 (a)	2.4E-05 ± 6.0E-06 (b)	4.0E-05 ± 8.8E-06 (c)	2.2E-04 ± 1.6E-04 (a,b,c)	0.0288
<i>IL8</i>	5.0E-04 ± 9.0E-05	2.5E-04 ± 2.0E-05	4.0E-04 ± 6.0E-05	9.1E-04 ± 5.9E-04	0.484
<i>IL10</i>	4.9E-04 ± 2.8E-05 (a)	3.9E-04 ± 1.7E-05	4.0E-04 ± 4.0E-05	2.9E-04 ± 3.6E-05 (a)	0.0132
<i>IL15</i>	2.1E-03 ± 8.8E-05	2.3E-03 ± 1.0E-04 (a)	2.1E-03 ± 1.3E-04	1.6E-03 ± 2.0E-04 (a)	0.0087
<i>LIF</i>	2.9E-05 ± 4.0E-06 (a)	2.0E-05 ± 3.0E-06 (b)	2.4E-05 ± 3.0E-06 (c)	9.2E-05 ± 3.1E-05 (a,b,c)	0.0007
<i>TGFβ</i>	6.3E-03 ± 6.0E-04 (a)	4.8E-03 ± 2.8E-04	6.0E-03 ± 5.0E-04 (b)	3.1E-03 ± 7.0E-04 (a,b)	0.0034
<i>TNFα</i>	3.5E-04 ± 2.6E-05 (a,b)	2.4E-04 ± 2.0E-05 (a)	3.1E-04 ± 2.0E-05 (c)	1.4E-04 ± 4.5E-05 (b,c)	0.0001
<i>GDF11</i>	2.5E-03 ± 2.5E-04 (a)	4.1E-03 ± 3.0E-04 (a,c)	4.0E-03 ± 2.5E-04 (a,c)	2.0E-03 ± 5.0E-04 (c)	0.0016
<i>FSTL1</i>	3.8E-04 ± 5.0E-05 (a)	3.2E-04 ± 2.4E-05 (b)	3.4E-04 ± 5.7E-05 (c)	9.0E-04 ± 2.6E-04 (a,b,c)	0.0011
<i>Irisin</i>	2.5E-02 ± 1.5E-03 (a)	2.6E-02 ± 1.3E-03 (b)	2.6E-02 ± 1.7E-03 (c)	9.7E-03 ± 1.9E-03 (a,b,c)	0.0001
<i>FGF21</i>	3.3E-04 ± 1.5E-05 (a)	6.9E-04 ± 1.5E-04 (a,b,c)	3.5E-04 ± 9.0E-05 (b)	2.5E-04 ± 3.8E-05 (c)	0.0159
<i>IGF-1</i>	1.1E-02 ± 9.0E-04 (a)	8.5E-03 ± 4.6E-04	8.6E-03 ± 5.3E-04	6.7E-03 ± 1.3E-03 (a)	0.0046
<i>Apelin</i>	1.9E-03 ± 1.6E-04 (a)	1.5E-03 ± 9.0E-05 (b)	1.6E-03 ± 1.6E-04 (c)	5.6E-04 ± 1.6E-04 (a,b,c)	0.0001

The table shows the ratios of different heart gene expression/*RPLPO* gene expression as a function of the CKD severity. The group mean values with the same letters (a, b, c) are significantly different.

CKD rats (Table 5). We detected a decrease in IGF-1, Apelin and Irisin expression (Table 5).

To search for biomarkers reflecting cardiac dysfunction or cardiac fibrosis, we performed Pearson linear correlations between, heart function, fibrosis and RNA expression, followed by variable clustering. We identified six clusters, and correlations are displayed as a heatmap (Fig. 7A). In cluster 1, we found a negative association between Irisin heart expression and the  $E/e'$  parameter (Fig. 7A and 7B), but also with Sirius red. This cardiokine is therefore negatively correlated with diastolic function and cardiac fibrosis. In contrast, galectin-3 is positively correlated with  $E/e'$  and cardiac fibrosis (Sirius red). sST2 expression is also negatively associated with Sirius red staining. As expected, we found in cluster 2 that EF was positively correlated with plasma creatinine concentration and BNP expression. In cluster 4, unsurprisingly, collagen 1 expression was associated with cardiac hypertrophy (LVPW, left ventricular posterior wall) and hypertension (SAP). Interestingly, ANP expression is correlated with heart fibrosis (Fig. 7A and 7C) and hypertrophy (LVPW and HW/BW parameters). We also found that IL-33 (Cluster 5) was positively correlated with the hypertrophy parameter LVPW and negatively correlated with EF. In cluster 6, we found that FGF23 was negatively associated with the hypertension (SAP, Systolic arterial pressure) while the receptor FGFR2 was negatively correlated with heart ejection fraction.

## Discussion

The study of cardiac function in patients and animal models of ARPKD has been limited. This study investigated ARPKD-related cardiac dysfunction

associated with CKD, highlighting the presence of type IV cardiorenal syndrome (CRS IV) (Guaricci et al., 2023). One limitation of this work is that only males were studied; however, females in this model rapidly develop liver damage, which would have interfered with cardio-renal syndrome development. CRS IV is characterized by CKD leading to the impairment of cardiac function (Clementi et al., 2013). This is consistent with our echocardiography investigation which demonstrated diastolic dysfunction rather than systolic impairment. Furthermore, molecular analysis highlighted the presence of cardiac fibrosis and cardiac remodelling, including a dysregulation of inflammatory and cardiokine pathways. Given the limited literature on cardiac dysfunctions in ARPKD patients, gaining a better understanding of the biological and molecular pathways at stake from animal models could benefit patients.

In line with other studies in ARPKD rat models, an increase in blood pressure and cardiac hypertrophy, specifically the thickening of the posterior wall, was observed in our study (Harrison et al., 2010; Lucchetti et al., 2023; Phillips et al., 2007). Additional studies analysing cardiac geometry in children with ARPKD showed a significantly impaired cardiac phenotype, characterized by abnormal left ventricular geometry coupled with systolic mechanical dysfunction (Chinali et al., 2019; Lucchetti et al., 2023). No modification of the global longitudinal strain was observed in our model and the alteration of ejection fraction appeared only in ARPKD 9M. Recently, dilated cardiomyopathy has been reported in a Japanese girl with ARPKD (Miura et al., 2020), while we did not observe left ventricular dilatation. Altogether, these observations confirm that a decrease in LVEF and LV dilatation are late findings

in uraemic cardiomyopathy (London et al., 2001) and especially in ARPKD. Previous studies have demonstrated abnormalities in myocardial function, including diastolic metrics (Chinali et al., 2019). In our model, we observed a decrease in diastolic velocity of mitral annular motion ( $e'$ ) and in mitral flow velocity ( $E/A$ ). The increase in  $E/e'$  ratio uncovers diastolic dysfunction, while alterations in LV relaxation are characteristic of cardio-renal syndrome IV (Mark et al., 2022). Diastolic dysfunction and heart failure with preserved ejection fraction (HFpEF) are associated with an increase in circulatory natriuretic peptides (Mark et al., 2022). Although we did not measure circulating ANP and BNP, heart ANP mRNA expression was found to be increased in ARPKD rats.

A recent study (Chinali et al., 2019) suggests the intriguing hypothesis that cardiac hypertrophy and systolic dysfunction in ARPKD might be not only a compensatory response to increased workload, but also a consequence of impaired myocardial contraction. However, in the early stages, we did not find strain and diastolic problems that would support this hypothesis. In our work, we found that diastolic dysfunction is associated with the severity of renal damage and with cardiac fibrosis and hypertrophy. However, hypertension does not appear to be a major factor in diastolic dysfunction. Various biomarkers such as Irisin, BNP, galectin-3 and GDF15 are correlated with diastolic dysfunction.

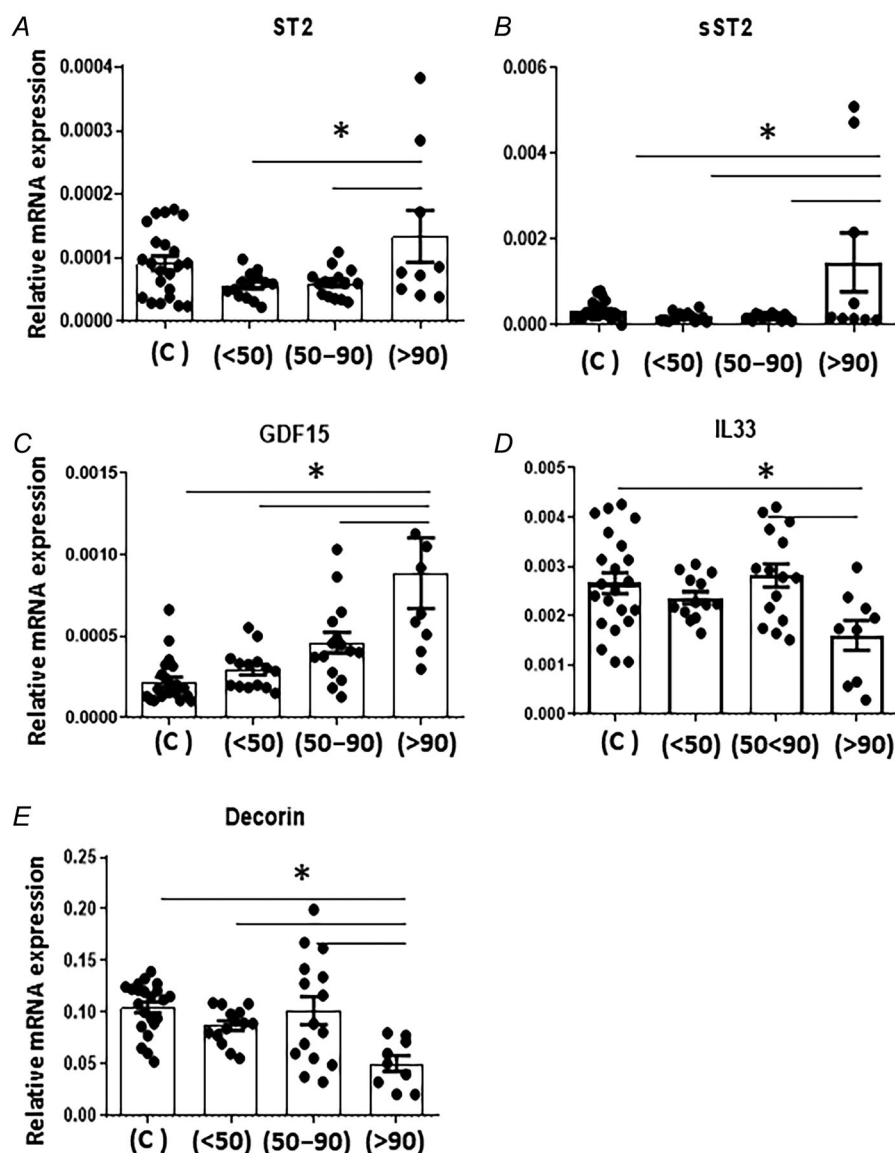


**Figure 6. Heart fibrosis signalling was activated in the ARPKD rats**

ST2 (A), sST2 (B), GDF15 (C), IL33 (D), and Decorin (E) gene expression in the heart as a function of the age or CKD severity. Gene expression was normalized to RPLPO expression. \*Significant difference,  $P < 0.05$ .



Multiple mechanisms contribute to the development of structural and functional cardiac abnormalities such as haemodynamic alterations, exposure to uraemic toxins, maladaptive neurohormonal response, endothelial dysfunction, CKD-induced systemic low-grade inflammation, cardiac fibrosis and chronic remodelling of myocardium (Gallo et al., 2023; Guaricci et al., 2023; Plawecki et al., 2018; Xanthopoulos et al., 2023). Consistent with the central role of low-grade inflammation, we observed increased heart inflammation with overexpression of IL-6 and decreased expression of the anti-inflammatory cytokine IL-10. Surprisingly, TGF- $\beta$  and TNF- $\alpha$  expression was reduced in the hearts in ARPKD rats, although this was previously reported in another model (Plawecki et al., 2024).

While cardiac fibrosis has been previously examined in the ARPKD model (Jeewandara et al., 2015; Sagar et al., 2019), this is the first study to demonstrate a relationship between the progression of heart fibrosis and kidney function decline. In severe kidney disease ARPKD, the observation of fibrosis through Sirius red staining and collagen-1 overexpression, along with fibrotic signalling molecules (galectin-3, sST2, GDF15), was consistent with previous clinical and preclinical studies (Fontana Estevez

et al., 2022; Plawecki et al., 2024). Interestingly, in severe ARPKD, there was an increase in ST2 and sST2, associated with a decrease in IL-33. Alarmin (IL-33) prevents cardiac inflammation and remodelling after its binding to its cell receptor, ST2 (Kuster et al., 2020). By contrast sST-2 acts as a decoy receptor and dramatically impairs the anti-inflammatory effects of IL-33. In severe chronic disease, a reduced IL-33/sST2 ratio could favour fibrotic processes. The potential involvement of profibrotic and remodelling factors was evaluated in our model. We first analysed FGF23 system expression in the heart. FGF23 is an endocrine hormone that regulates phosphate and calcium metabolism by reducing phosphate tubular reabsorption and by decreasing the levels of the active form of vitamin D. This renal action is secondary to its binding to the FGF23 receptor (FGFR) and its co-receptor Klotho (Edmonston et al., 2024). In addition, FGF23 appears as a main regulator implicated in left ventricular hypertrophy and premature mortality. The hypertrophic effects of FGF23 are mediated by the activation of cardiac FGFR4, a Klotho-independent receptor, resulting in the activation of the calcineurin/nuclear factor of activated T cells (NFAT) signalling cascade (Böckmann et al., 2019). In agreement with these data, we found a clear increase

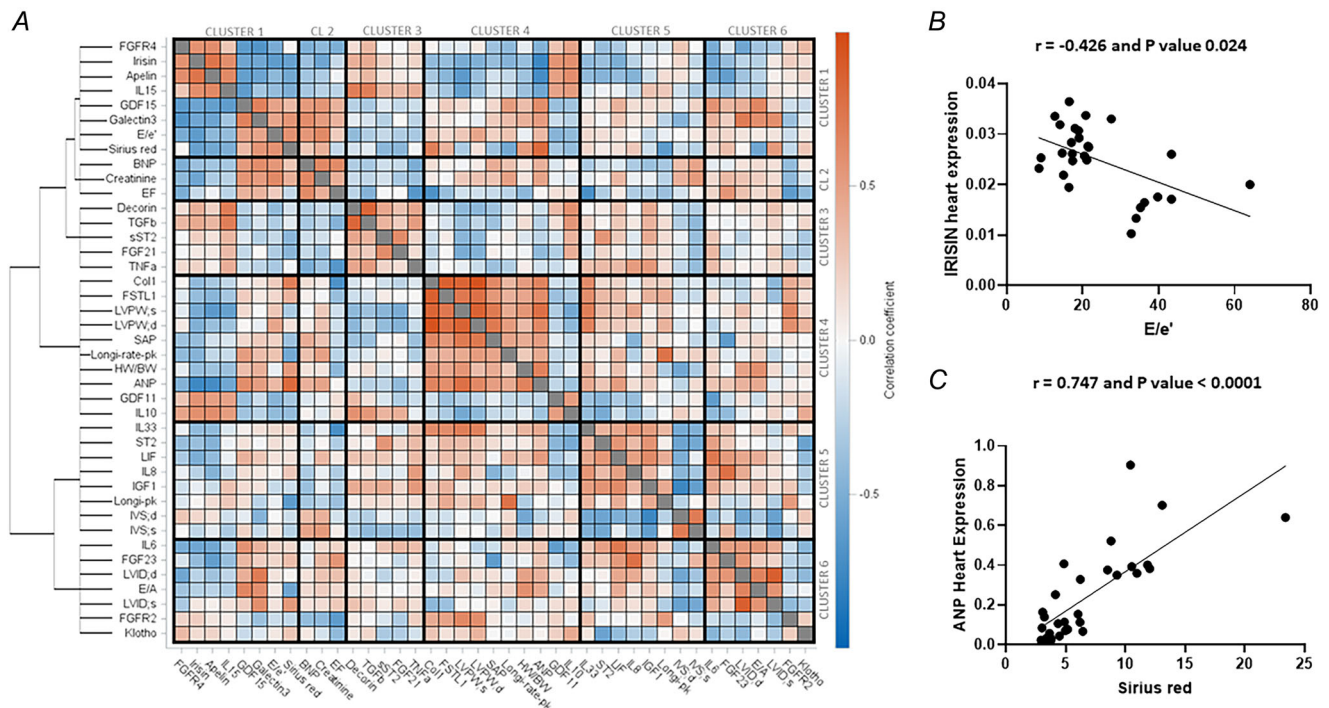


**Figure 7. Pearson correlation heatmap of markers of cardiac and renal functions in ARPKD rats**

A, we performed Pearson linear correlations between echocardiography, heart RNA expressions and markers, followed by variable clustering in 36 ARPKD rats (animals with echocardiography). Correlations are displayed as a heatmap where values are represented by coloured gradient of red (1) to blue (−1) and variables are organized according to the clustering dendrogram. B, non-parametric Spearman correlation test show that heart Irisin expression is correlated with decreased diastolic function ( $E/e'$  parameter). C, non-parametric Spearman correlation test show that ANP expression is correlated with heart fibrosis (Sirius red). [Colour figure can be viewed at [wileyonlinelibrary.com](http://wileyonlinelibrary.com)]



in FGF23 expression with CKD severity without changes in heart Klotho gene expression. Since animal models of klotho deficiency develop LVH and cardiac fibrosis (Hu et al., 2015), it has been suggested that Klotho could protect the heart against fibrosis. However, clinical research has produced conflicting data (Tanaka et al., 2016). In our ARPKD animal model, the clear imbalance of FGF23 and Klotho expression in the heart was in favour of cardiac fibrosis and remodelling. We did not observe any changes in FGFR4 expression in ARPKD animals, but interestingly, the expression of FGFR2 decreased with CKD severity. A recent study suggested that during ischaemia–reperfusion injury, FGFR1 and FGFR2 confer cardiomyocyte protection by reducing cell death and limiting hypertrophy (Matsiukevich et al., 2022). Therefore, a reduction in the expression of FGFR1 and FGFR2 in ARPKD animals is in favour of cardiac hypertrophy and fibrosis (Jeong et al., 2023).

Cardiokines expression was analysed to explore the secretory pathway dysregulation. The expression of growth/differentiation factor-15 (GDF15), which is known to be overexpressed during cardiac damage and to act as a cardioprotective agent (Wesseling et al., 2020), increased progressively with CKD and fibrosis severity. GDF15 has recently been identified as a possible inhibitor of fibroblast growth by repressing TGF- $\beta$  signalling (Wesseling et al., 2020). The increase in its heart expression during CKD-induced heart failure is consistent with the high levels of GDF15 observed in clinical studies (Kuster et al., 2020). In addition, Decorin, which inhibits the fibrotic action of TGF- $\beta$ 1 (Alan et al., 2011), is significantly decreased in animals with severe CKD. These results confirm the impairment of signalling pathways involved in preventing heart fibrosis.

GDF11 and FGF21 have also been shown to protect against cardiac hypertrophy (Harper et al., 2018; Planavila et al., 2015) and here again their expression was increased in the first stage of CKD. FSTL1, a protein that appears to have a cardioprotective role and attenuates hypertrophy following pressure overload (Shimano et al., 2011), showed overexpression in animals with severe CKD (Table 5). We detected a decrease in IGF-1 expression, which is also involved in heart hypertrophy (Bass-Stringer et al., 2021). As previously reported in hypertension development (Schnelle et al., 2018), Apelin gene expression was decreased in animals with severe CKD and pressure overload (Table 5). We also observed a decrease in gene expression of Irisin, a protein implicated in heart metabolism and oxidative stress regulation, in rats with severe CKD. Interestingly, Irisin expression was negatively correlated with the echocardiographic parameter  $E/e'$  (Fig. 7B), indicating a relationship with diastolic dysfunction, in agreement with a previous report by Huerta-Delgado et al. (2022). Irisin could be a good biomarker of cardiac diastolic damage.

The dysregulation of cardiokine expression, including GDF15, GDF11, FSTL1, FGF21, Decorin, Apelin and Irisin, highlights significant abnormalities in heart secretory function involved in fibrosis, hypertrophy and cardiac metabolism.

In conclusion, this study represents the first large exploration of heart function and signalling in an ARPKD model. Our findings reveal the presence of heart diastolic dysfunction and fibrosis, which are correlated with kidney dysfunction. The dysregulation of cytokine and cardiokine signalling pathways during CKD progression likely contributes to heart dysfunction and the progression of cardiac pathology in ARPKD. These findings shed light on the complex interplay between kidney and heart in ARPKD. Further studies are needed to elucidate the underlying mechanisms and to develop targeted treatments to improve cardiovascular outcomes in ARPKD patients.

## References

- Alan, C., Kocoglu, H., Altıntas, R., Alici, B., & Resit Ersay, A. (2011). Protective effect of decorin on acute ischaemia-reperfusion injury in the rat kidney. *Archives of Medical Science*, **2**, 211–216.
- Anon. (2013). Notice. *Kidney International Supplements*, **3**(1), 1.
- Bass-Stringer, S., Tai, C. M. K., & McMullen, J. R. (2021). IGF1-PI3K-induced physiological cardiac hypertrophy: Implications for new heart failure therapies, biomarkers, and predicting cardiotoxicity. *Journal of Sport and Health Science*, **10**(6), 637–647.
- Benz, E. G., & Hartung, E. A. (2021). Predictors of progression in autosomal dominant and autosomal recessive polycystic kidney disease. *Pediatric Nephrology*, **36**(9), 2639–2658.
- Bergmann, C., Frank, V., Küpper, F., Kamitz, D., Hanten, J., Berges, P., Mager, S., Moser, M., Kirfel, J., Büttner, R., Senderek, J., & Zerres, K. (2006). Diagnosis, pathogenesis, and treatment prospects in cystic kidney disease. *Molecular Diagnosis & Therapy*, **10**(3), 163–174.
- Bergmann, C., Senderek, J., Küpper, F., Schneider, F., Dornia, C., Windelen, E., Eggermann, T., Rudnik-Schöneborn, S., Kirfel, J., Furu, L., Onuchic, L. F., Rossetti, S., Harris, P. C., Somlo, S., Guay-Woodford, L., Germino, G. G., Moser, M., Büttner, R., & Zerres, K. (2004). *PKHD1* mutations in autosomal recessive polycystic kidney disease (ARPKD). *Human Mutation*, **23**(5), 453–463.
- Böckmann, I., Lischka, J., Richter, B., Deppe, J., Rahn, A., Fischer, D.-C., Heineke, J., Haffner, D., & Leifheit-Nestler, M. (2019). FGF23-Mediated activation of local RAAS promotes cardiac hypertrophy and fibrosis. *International Journal of Molecular Sciences*, **20**(18), 4634.
- Capisonda, R., Phan, V., Traubci, J., Daneman, A., Balfe, J. W., & Guay-Woodford, L. M. (2003). Autosomal recessive polycystic kidney disease: Outcomes from a single-center experience. *Pediatric Nephrology*, **18**(2), 119–126.

- Castiglione, V., Aimò, A., Vergaro, G., Saccaro, L., Passino, C., & Emdin, M. (2022). Biomarkers for the diagnosis and management of heart failure. *Heart Failure Reviews*, **27**(2), 625–643.
- Chinali, M., Lucchetti, L., Ricotta, A., Esposito, C., D'Anna, C., Rinelli, G., Emma, F., & Massella, L. (2019). Cardiac abnormalities in children with autosomal recessive polycystic kidney disease. *Cardiorenal Medicine*, **9**(3), 180–189.
- Chinali, M., Matteucci, M. C., Franceschini, A., Doyon, A., Pongiglione, G., Rinelli, G., & Schaefer, F. (2015). Advanced parameters of cardiac mechanics in children with CKD: The 4C study. *Clinical Journal of the American Society of Nephrology*, **10**(8), 1357–1363.
- Chinali, M., de Simone, G., Matteucci, M. C., Picca, S., Mastrostefano, A., Anarat, A., Caliskan, S., Jeck, N., Neuhaus, T. J., Peco-Antic, A., Peruzzi, L., Testa, S., Mehls, O., Wühl, E., Schaefer, F., & ESCAPE Trial Group. (2007). Reduced systolic myocardial function in children with chronic renal insufficiency. *Journal of the American Society of Nephrology*, **18**(2), 593–598.
- Clementi, A., Virzi, G. M., Goh, C. Y., Cruz, D. N., Granata, A., Vescovo, G., & Ronco, C. (2013). Cardiorenal syndrome type 4: A review. *Cardiorenal Medicine*, **3**(1), 63–70.
- Edmonston, D., Grabner, A., & Wolf, M. (2024). FGF23 and klotho at the intersection of kidney and cardiovascular disease. *Nature Reviews Cardiology*, **21**(1), 11–24.
- El-Armouche, A., Ouchi, N., Tanaka, K., Doros, G., Wittköpper, K., Schulze, T., Eschenhagen, T., Walsh, K., & Sam, F. (2011). Follistatin-like 1 in chronic systolic heart failure: A marker of left ventricular remodeling. *Circulation: Heart Failure*, **4**, 621–627.
- Field, M. L. (1985). Low-renin hypertension in young infants. *Archives of Pediatrics & Adolescent Medicine*, **139**(8), 823.
- Fontana Estevez, F. S., Betazza, M. C., Mikszutowicz, V., Seropian, I. M., Silva, M. G., Penas, F., Touceda, V., Selser, C., Villaverde, A., Goren, N., Cianciulli, T. F., Medina, V., Morales, C., Gironacci, M., & González, G. E. (2022). Genetic deletion of Galectin-3 exacerbates age-related myocardial hypertrophy and fibrosis in mice. *Cellular Physiology and Biochemistry*, **56**, 353–366.
- Furukawa, N., Koitabashi, N., Matsui, H., Sunaga, H., Umbarawan, Y., Syamsunarno, M., Yamaguchi, A., Obokata, M., Hanaoka, H., Yokoyama, T., & Kurabayashi, M. (2021). DPP-4 inhibitor induces FGF21 expression via sirtuin 1 signaling and improves myocardial energy metabolism. *Heart and Vessels*, **36**(1), 136–146.
- Gabow, P. A., Chapman, A. B., Johnson, A. M., Tangel, D. J., Duley, I. T., Kaehny, W. D., Manco-Johnson, M., & Schrier, R. W. (1990). Renal structure and hypertension in autosomal dominant polycystic kidney disease. *Kidney International*, **38**(6), 1177–1180.
- Gagnadoux, M. F., Habib, R., Levy, M., Brunelle, F., & Broyer, M. (1989). Cystic renal diseases in children. *Advances in Nephrology from the Necker Hospital*, **18**, 33–57.
- Gallo, G., Lanza, O., & Savoia, C. (2023). New insight in cardiorenal syndrome: From biomarkers to therapy. *International Journal of Molecular Sciences*, **24**(6), 5089.
- Guaricci, A. I., Sturdà, F., Russo, R., Basile, P., Baggiano, A., Mushtaq, S., Fusini, L., Fazzari, F., Bertandino, F., Monitillo, F., Carella, M. C., Simonini, M., Pontone, G., Ciccone, M. M., Grandaliano, G., Vezzoli, G., & Pesce, F. (2023). Assessment and management of heart failure in patients with chronic kidney disease. *Heart Failure Reviews*, **29**(2), 379–394.
- Harper, S. C., Johnson, J., Borghetti, G., Zhao, H., Wang, T., Wallner, M., Kubo, H., Feldsott, E. A., Yang, Y., Joo, Y., Gou, X., Sabri, A. K., Gupta, P., Myzithras, M., Khalil, A., Franti, M., & Houser, S. R. (2018). GDF11 Decreases pressure overload-induced hypertrophy, but can cause severe cachexia and premature death. *Circulation Research*, **123**(11), 1220–1231.
- Harris, P. C., & Torres, V. E. (2009). Polycystic kidney disease. *Annual Review of Medicine*, **60**(1), 321–337.
- Harrison, J. L., Hildreth, C. M., Callahan, S. M., Goodchild, A. K., & Phillips, J. K. (2010). Cardiovascular autonomic dysfunction in a novel rodent model of polycystic kidney disease. *Autonomic Neuroscience*, **152**(1–2), 60–66.
- Hu, M. C., Shi, M., Cho, H. J., Adams-Huet, B., Paek, J., Hill, K., Shelton, J., Amaral, A. P., Faul, C., Taniguchi, M., Wolf, M., Brand, M., Takahashi, M., Kuro-O, M., Hill, J. A., & Moe, O. W. (2015). Klotho and phosphate are modulators of pathologic uremic cardiac remodeling. *Journal of the American Society of Nephrology*, **26**(6), 1290–1302.
- Huerta-Delgado, A. S., Roffe-Vazquez, D. N., Luna-Ceron, E., Gonzalez-Gil, A. M., Casillas-Fikentscher, A., Villarreal-Calderon, J. R., Enriquez, C., de la Peña-Almaguer, E., Castillo, E. C., Silva-Platas, C., Garcia-Rivas, G., & Elizondo-Montemayor, L. (2022). Association of irisin levels with cardiac magnetic resonance, inflammatory, and biochemical parameters in patients with chronic heart failure versus controls. *Magnetic Resonance Imaging*, **93**, 62–72.
- Jeewandara, T. M., Ameer, O. Z., Boyd, R., Wyse, B. F., Underwood, C. F., & Phillips, J. K. (2015). Protective cardiorenal effects of spironolactone in a rodent model of polycystic kidney disease. *Clinical and Experimental Pharmacology and Physiology*, **42**(4), 353–360.
- Jeong, A., Lim, Y., Kook, T., Kwon, D. H., Cho, Y. K., Ryu, J., Lee, Y. G., Shin, S., Choe, N., Kim, Y. S., Cho, H. J., Kim, J. C., Choi, Y., Lee, S. J., Kim, H. S., Kee, H. J., Nam, K. I., Ahn, Y., Jeong, M. H., Park, W. J., ... Kook, H. (2023). Circular RNA circSMAD4 regulates cardiac fibrosis by targeting miR-671-5p and FGFR2 in cardiac fibroblasts. *Molecular Therapy Nucleic Acids*, **34**, 102071.
- Kaplan, B. S., Fay, J., Shah, V., Dillon, M. J., & Martin Barratt, T. (1989). Autosomal recessive polycystic kidney disease. *Pediatric Nephrology*, **3**(1), 43–49.
- Klein, J., Caubet, C., Camus, M., Makridakis, M., Denis, C., Gilet, M., Feuillet, G., Rascalou, S., Neau, E., Garrigues, L., Thillaye du Boullay, O., Mischak, H., Monsarrat, B., Burlet-Schiltz, O., Vlahou, A., Saulnier-Blache, J. S., Bascands, J.-L., & Schanstra, J. P. (2020). Connectivity mapping of glomerular proteins identifies dimethylaminoparthenolide as a new inhibitor of diabetic kidney disease. *Scientific Reports*, **10**(1), 14898.

- Kuster, N., Huet, F., Dupuy, A.-M., Akodad, M., Battistella, P., Agullo, A., Leclercq, F., Kalmanovich, E., Meilhac, A., Aguilhon, S., Cristol, J.-P., & Roubille, F. (2020). Multimarker approach including CRP, sST2 and GDF-15 for prognostic stratification in stable heart failure. *European Society of Cardiology Heart Failure*, 7(5), 2230–2239.
- Lager, D. J., Qian, Q., Bengal, R. J., Ishibashi, M., & Torres, V. E. (2001). The pck rat: A new model that resembles human autosomal dominant polycystic kidney and liver disease. *Kidney International*, 59(1), 126–136.
- Lindsey, M. L., Kassiri, Z., Virag, J. A. I., de Castro Brás, L. E., & Scherrer-Crosbie, M. (2018). Guidelines for measuring cardiac physiology in mice. *American Journal of Physiology-Heart and Circulatory Physiology*, 314(4), H733–H752.
- London, G. M., Pannier, B., Guerin, A. P., Blacher, J., Marchais, S. J., Darne, B., Metivier, F., Adda, H., & Safar, M. E. (2001). Alterations of left ventricular hypertrophy in and survival of patients receiving hemodialysis: Follow-up of an interventional study. *Journal of the American Society of Nephrology*, 12(12), 2759–2767.
- Lucchetti, L., Chinali, M., Emma, F., & Massella, L. (2023). Autosomal dominant and autosomal recessive polycystic kidney disease: Hypertension and secondary cardiovascular effect in children. *Frontiers in Molecular Biosciences*, 10, 1112727.
- Mark, P. B., Mangion, K., Rankin, A. J., Rutherford, E., Lang, N. N., Petrie, M. C., Stoumpos, S., & Patel, R. K. (2022). Left ventricular dysfunction with preserved ejection fraction: The most common left ventricular disorder in chronic kidney disease patients. *Clinical Kidney Journal*, 15(12), 2186–2199.
- Matsiukevich, D., House, S. L., Weinheimer, C., Kovacs, A., & Ornitz, D. M. (2022). Fibroblast growth factor receptor signaling in cardiomyocytes is protective in the acute phase following ischemia-reperfusion injury. *Frontiers in Cardiovascular Medicine*, 9, 1011167.
- Miura, A., Kondo, H., Yamamoto, T., Okumura, Y., & Nishio, H. (2020). Sudden unexpected death of infantile dilated cardiomyopathy with JPH2 and PKD1 gene variants. *International Heart Journal*, 61(5), 1079–1083.
- Pfaffl, M. W. (2001). A new mathematical model for relative quantification in real-time RT-PCR. *Nucleic Acids Research*, 29(9), 45e–45.
- Phillips, J. K., Hopwood, D., Loxley, R. A., Ghatora, K., Coombes, J. D., Tan, Y. S., Harrison, J. L., McKittrick, D. J., Holobotsky, V., Arnold, L. F., & Rangan, G. K. (2007). Temporal relationship between renal cyst development, hypertension and cardiac hypertrophy in a new rat model of autosomal recessive polycystic kidney disease. *Kidney & Blood Pressure Research*, 30(3), 129–144.
- Planavila, A., Redondo-Angulo, I., & Villarroja, F. (2015). FGF21 and cardiac physiopathology. *Frontiers in Endocrinology (Lausanne)*, 6, 133.
- Plawecki, M., Gayrard, N., Jeanson, L., Chauvin, A., Lajoix, A.-D., Cristol, J.-P., Jover, B., & Raynaud, F. (2024). Cardiac remodeling associated with chronic kidney disease is enhanced in a rat model of metabolic syndrome: Preparation of mesenchymal transition. *Molecular and Cellular Biochemistry*, 479(1), 29–39.
- Plawecki, M., Morena, M., Kuster, N., Chenine, L., Leray-Moragues, H., Jover, B., Fesler, P., Lotierzo, M., Dupuy, A.-M., Klouche, K., & Cristol, J.-P. (2018). sST2 as a new biomarker of chronic kidney disease-induced cardiac remodeling: Impact on risk prediction. *Mediators of Inflammation*, 2018, 1–9.
- Sagar, P. S., Zhang, J., Luciuk, M., Mannix, C., Wong, A. T. Y., & Rangan, G. K. (2019). Increased water intake reduces long-term renal and cardiovascular disease progression in experimental polycystic kidney disease. *PLoS ONE*, 14(1), e0209186.
- Schnelle, M., Catibog, N., Zhang, M., Nabeebaccus, A. A., Anderson, G., Richards, D. A., Sawyer, G., Zhang, X., Toischer, K., Hasenfuss, G., Monaghan, M. J., & Shah, A. M. (2018). Echocardiographic evaluation of diastolic function in mouse models of heart disease. *Journal of Molecular and Cellular Cardiology*, 114, 20–28.
- Shimano, M., Ouchi, N., Nakamura, K., van Wijk, B., Ohashi, K., Asaumi, Y., Higuchi, A., Pimentel, D. R., Sam, F., Murohara, T., van den Hoff, M. J. B., & Walsh, K. (2011). Cardiac myocyte follistatin-like 1 functions to attenuate hypertrophy following pressure overload. *Proceedings of the National Academy of Sciences, USA*, 108(43), E899–E906.
- Sicard, P., Jouitteau, T., Andrade-Martins, T., Massad, A., Rodrigues de Araujo, G., David, H., Miquerol, L., Colson, P., & Richard, S. (2019). Right coronary artery ligation in mice: A novel method to investigate right ventricular dysfunction and biventricular interaction. *American Journal of Physiology-Heart and Circulatory Physiology*, 316(3), H684–H692.
- Tanaka, S., Fujita, S.-I., Kizawa, S., Morita, H., & Ishizaka, N. (2016). Association between FGF23,  $\alpha$ -klotho, and cardiac abnormalities among patients with various chronic kidney disease stages. *PLoS ONE*, 11(7), e0156860.
- Turkbey, B., Ocak, I., Daryanani, K., Font-Montgomery, E., Lukose, L., Bryant, J., Tuchman, M., Mohan, P., Heller, T., Gahl, W. A., Choyke, P. L., & Gunay-Aygun, M. (2009). Autosomal recessive polycystic kidney disease and congenital hepatic fibrosis (ARPKD/CHF). *Pediatric Radiology*, 39(2), 100–111.
- Walker, R. V., Yao, Q., Xu, H., Maranto, A., Swaney, K. F., Ramachandran, S., Li, R., Cassina, L., Polster, B. M., Outeda, P., Boletta, A., Watnick, T., & Qian, F. (2023). Fibrocystin/polyductin releases a C-terminal fragment that translocates into mitochondria and suppresses cystogenesis. *Nature Communications*, 14(1), 6513.
- Wesseling, M., de Poel, J. H. C., & de Jager, S. C. A. (2020). Growth differentiation factor 15 in adverse cardiac remodelling: From biomarker to causal player. *European Society of Cardiology Heart Failure*, 7(4), 1488–1501.

- Xanthopoulos, A., Papamichail, A., Briasoulis, A., Loritis, K., Bourazana, A., Magouliotis, D. E., Sarafidis, P., Stefanidis, I., Skoularigis, J., & Triposkiadis, F. (2023). Heart failure in patients with chronic kidney disease. *Journal of Clinical Medicine*, **12**(18), 6105.
- Zerres, K., Mücher, G., Becker, J., Steinkamm, C., Rudnik-Schöneborn, S., Heikkilä, P., Rapola, J., Salonen, R., Germino, G. G., Onuchic, L., Somlo, S., Avner, E. D., Harman, L. A., Stockwin, J. M., & Guay-Woodford, L. M. (1998). Prenatal diagnosis of autosomal recessive polycystic kidney disease (ARPKD): Molecular genetics, clinical experience, and fetal morphology. *American Journal of Medical Genetics*, **76**(2), 137–144.
- Zouein, F. A., Kurdi, M., & Booz, G. W. (2013). LIF and the heart: Just another brick in the wall? *European Cytokine Network*, **24**, 11–19.

## Additional information

### Data availability statement

The data supporting these results in the paper are available from the corresponding author upon request.

### Competing interests

The authors declare that there is no conflict of interest regarding the publication of this paper.

### Author contributions

Conception or design of the work, N.G., J.P.C. and F.R. Acquisition, analysis or interpretation of data for the work

methodology, N.G., M.P., C.L., F.D., M.F., P.S., I.C.T., M.L., B.J., J.P.C. and F.R. Drafting the work or revising it critically for important intellectual content, N.G., J.H.B., B.J., J.P.C. and F.R. All authors have read and approved the final version of this manuscript and agree to be accountable for all aspects of the work in ensuring that questions related to the accuracy or integrity of any part of the work are appropriately investigated and resolved. All persons designated as authors qualify for authorship, and all those who qualify for authorship are listed.

### Funding

SFNDT: F.R., IRCT dialysis 2023.

### Acknowledgements

The authors thank the Société Francophone de Néphrologie (SFNDT) for its support and Montpellier's histology platform, the RHEM-Biocampus, for their technical assistance.

### Keywords

ARPKD, chronic kidney disease, diastolic function, heart fibrosis and cardiokines

## Supporting information

Additional supporting information can be found online in the Supporting Information section at the end of the HTML view of the article. Supporting information files available:

### Peer Review History